EARTHQUAKE ENGINEERING AND STRUCTURAL DYNAMICS
Earthquake Engng Struct. Dyn. 2006; **35**:177–197
Published online 1 September 2005 in Wiley InterScience (www.interscience.wiley.com). DOI: 10.1002/eqe.514

Seismic response control of smart sliding isolated buildings using variable stiffness systems: An experimental and numerical study

Satish Nagarajaiah[1,*,†,‡] and Sanjay Sahasrabudhe[1,2]

[1]*Departments of Civil and Environmental Engineering, and Mechanical Engineering and Material Science, Rice University, Houston, TX 77005, U.S.A.*
[2]*Structural Engineering Department, J Ray McDermott Engineering LLC, Houston, TX 77079, U.S.A.*

SUMMARY

Effectiveness of a new semiactive independently variable stiffness (SAIVS) device in reducing seismic response of sliding base isolated buildings is evaluated analytically and experimentally. Through analytical and experimental study of force—displacement behaviour of the SAIVS device, it is shown that the device can vary stiffness continuously and smoothly between minimum and maximum stiffness. Passive sliding base isolation systems reduce interstorey drifts and superstructure accelerations, but with increased base displacements, which is undesirable, under large velocity near fault pulse type earthquakes. It is a common practice to incorporate non-linear passive dampers into the isolation system to reduce bearing displacements. Incorporation of passive dampers, however, may result in increased superstructure accelerations and drifts; while, properly designed passive dampers can be beneficial. A viable alternative is to use semiactive variable stiffness systems, which can vary the period of the sliding base isolated buildings in real time, to simultaneously reduce bearing displacements and superstructure responses further than the passive systems, which deserves investigation. This study investigates the performance of a 1:5 scaled smart sliding base isolated building model equipped with the SAIVS device analytically and experimentally, under near fault earthquakes, by developing a new moving average non-linear tangential stiffness control algorithm for control of the SAIVS device. The SAIVS device reduces bearing displacements further than the passive cases, while maintaining isolation level forces and superstructure responses at the same level as the passive minimum stiffness case, indicating the significant potential of the SAIVS system. Copyright © 2005 John Wiley & Sons, Ltd.

KEY WORDS: buildings; sliding base isolation; near fault earthquakes; variable stiffness; semiactive control; seismic response

*Correspondence to: Satish Nagarajaiah, Departments of Civil and Environmental Engineering, and Mechanical Engineering and Material Science, Rice University, Houston, TX 77005, U.S.A.
†E-mail: nagaraja@rice.edu
‡Associate Professor.

Contract/grant sponsor: National Science Foundation; contract/grant number: CMS-9996290

Received 8 January 2005
Revised 10 May 2005
Accepted 1 June 2005

INTRODUCTION

Sliding isolation systems are effective in reducing seismic response of buildings under near fault earthquakes [1, 2]. In buildings, sliding base isolation systems reduce interstorey drifts and superstructure accelerations; but at an expense of increased bearing displacements. Under near fault, large velocity pulse type earthquakes, such increase in bearing displacements is undesirable [3, 4]. To reduce bearing displacements, it is a common practice to incorporate non-linear passive dampers into the isolation system [5]. Passive dampers may result in increased interstorey drifts and superstructure accelerations [6]; however, properly designed dampers can be beneficial [7, 8]. Semiactive variable stiffness systems, which can vary the stiffness of the sliding base isolation systems in real time, may reduce bearing displacements and superstructure responses further than the passive systems; hence, deserve investigation.

Base isolation systems which utilize semiactive controllable devices are known as smart base isolation systems. A variety of passive, active, and semiactive devices, for seismic response reduction, have been proposed [9]. Nagarajaiah [10] proposed the use of semiactive dampers in base isolated structures, and showed their effectiveness in reducing seismic response. The applications of semiactive magneto-rheological (MR) fluid dampers [11, 12], in reducing seismic response of smart elastomeric base isolated buildings have been studied analytically [13, 14] and experimentally [15], and shown to be effective. The effectiveness of MR dampers in sliding base isolated buildings [16] and bridges [17] has been studied analytically and experimentally. The effectiveness of semiactive electro-rheological (ER) dampers, in reducing seismic response of elastomeric base isolated buildings has been studied analytically [18, 19], and shown to be effective. The application of variable orifice fluid dampers in elastomeric base isolated buildings [20, 21] and bridges [22] and in sliding base isolated buildings [23] has been studied analytically. Nagarajaiah *et al.* [24] experimentally studied applications of active hydraulic actuators in sliding base isolated bridges, controlled using an absolute acceleration feedback, and showed their effectiveness. However, large power requirement of active systems is a limiting factor in seismic applications.

An active variable stiffness (AVS) system, for seismic response control in buildings, has been developed by Kobori *et al.* [25]. The AVS system changes building stiffness by engaging and disengaging the braces in each storey of the structural framing system. It has been implemented in a full scale structure in Tokyo, Japan. Performance of the AVS system in reducing seismic response has been studied analytically [26] and shown to be effective in reducing response. One of the limitations of the AVS system is the on–off type stiffness switching, which results in sudden changes in stiffness, and corresponding increased structural response [25]. Yang *et al.* [27] analytically studied applications of on–off type resetting stiffness dampers [28] in elastomeric base isolated buildings, and showed its effectiveness. In order to overcome the limitations of conventional on–off type variable stiffness systems, a new semiactive independently variable stiffness (SAIVS) device has been developed [29]. The SAIVS device is capable of changing the stiffness continuously and smoothly between minimum and maximum stiffness. Nagarajaiah *et al.* [29] experimentally studied the effectiveness of a small scale SAIVS device in a single degree of freedom system, and demonstrated that by switching the stiffness continuously and smoothly a non-resonant state can be achieved; thus, reducing both the displacement and acceleration response. Narasimhan and Nagarajaiah [30] analytically studied application of the SAIVS device in a linear elastomeric base isolated reinforced concrete building, and showed its effectiveness. The main objective of this study

is to evaluate the effectiveness of semiactive variable stiffness systems in reducing seismic response of sliding base isolated buildings; since, it has not been evaluated.

Analytical and experimental study of a 1:5 scaled steel two-storey sliding base isolated (Teflon®-stainless steel bearings) building model, equipped with an SAIVS device is presented in this paper. The SAIVS device is incorporated into the sliding isolation system of the building model. The force–displacement characteristics of the SAIVS device are studied analytically and experimentally and it is shown that the SAIVS device is capable of varying the stiffness continuously and smoothly, between minimum and maximum stiffness. An analytical model of the building, which includes the non-linear characteristics of the sliding bearings and SAIVS device, is developed. Responses of the building model under variety of near fault earthquakes are computed using the analytical model, and a new control algorithm for control of the SAIVS device. Shake table tests are performed using several near fault earthquakes. Analytical and experimental results are compared [31]. The SAIVS device in the semiactive controlled mode reduces the bearing displacements further than the passive minimum and passive maximum stiffness cases, while maintaining isolation level forces, interstorey drifts, and superstructure accelerations close to the passive minimum stiffness case, indicating the significant potential of the SAIVS system.

SEMI-ACTIVE INDEPENDENTLY VARIABLE STIFFNESS (SAIVS) DEVICE

The SAIVS device consists of four springs (each 15.24 cm long) arranged in a rhombus configuration as shown in Figure 1(a). Each spring is located at an angle θ to the horizontal. Each of the four springs is supported on the inside by two telescoping tubes, which allow extension and compression of the springs and prevent them from buckling. The telescoping tubes contribute to the frictional forces in the device, which adds energy dissipation characteristics. As shown in Figure 1(a), an electromechanical actuator controlled with a computer is connected to joint 1. Joint 1 is fixed in the X direction and can be positioned in any desired position in the Y direction by the attached actuator and controller, thus changing θ. Joint 2 is free to move in the X and Y directions. Joints 3 and 4 are free to move in the X direction only. The guide rail, on which joint 2 moves, is attached to the shake table. The guide rails, on which joints 3 and 4 move, are attached to the base. The electromechanical actuator is fixed to the base and can move joint 1 to the any position in the Y direction, as desired. Thus, the electromechanical actuator can switch the configuration the SAIVS device to any desired position continuously and smoothly by positioning joint 1. Depending on its current position, the device generates connection force at joint 1 in the X direction, due to the relative displacement between joints 1 and 2. The device in the passive open and passive closed positions is shown in Figures 1(b) and (c), respectively. In the open position (Figure 1(b)), the device offers minimum resistance and has minimum stiffness. In the closed position (Figure 1(c)), the device offers maximum resistance and has maximum stiffness. Using the electromechanical actuator, the device can also be switched to any configuration in between open and closed positions. Hence, the device is capable of varying the stiffness continuously and smoothly between the minimum and maximum stiffness. The actuator requires 104 W peak power, and voltage supply in the range of 0–4 V to change the configuration of the device from open to closed position. The device does not move in the Z direction.

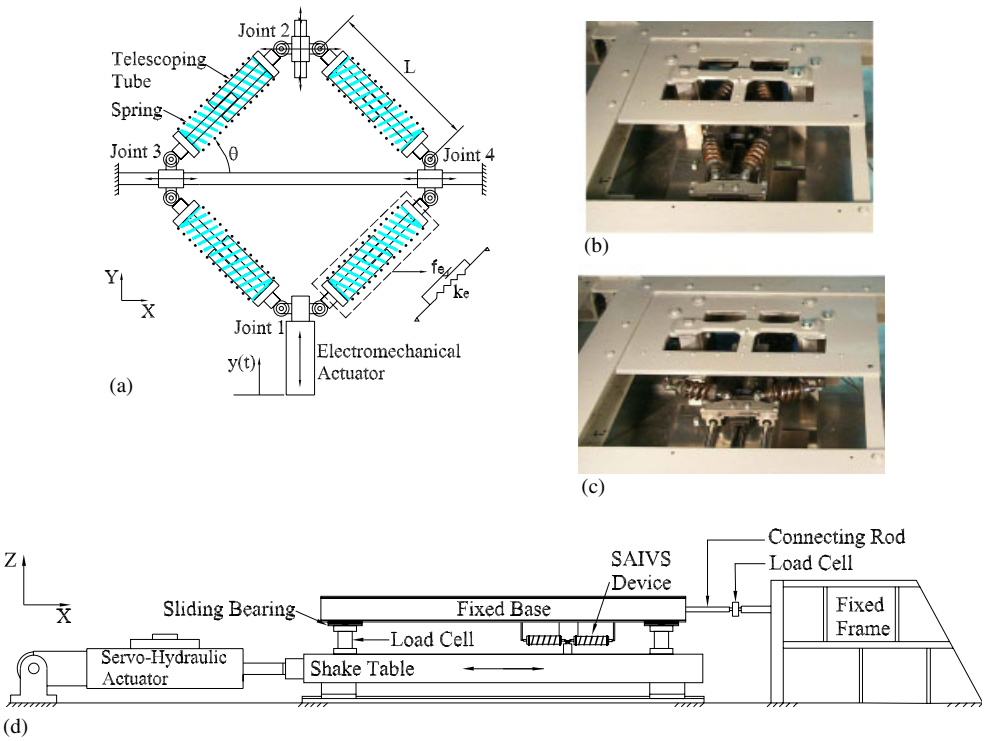

Figure 1. Semi-active independently variable stiffness (SAIVS) device: (a) analytical model; (b) device in open position; (c) device in closed position; and (d) calibration setup.

Analytical model of the SAIVS device

Analytical model of the SAIVS device, shown in Figure 1(a), consists of four sets of spring and friction elements arranged in a rhombus configuration. The friction elements represent the friction in the telescoping tubes. Each spring and friction element in the device is located at an angle θ, to the horizontal. This time varying angle θ is computed using the device position in the Y direction, which is monitored by connecting a linear variable displacement transducer (LVDT) to joint 1. Thus for any specific device position, the force in the device consists of forces due to the spring elements and the friction elements, which is:

$$F(t,u,\dot{u}) = F_{\mathrm{r}}(t) + F_{\mathrm{f}}(t,\dot{u}) \tag{1}$$

where F_{r} is the restoring force due to spring deformation, F_{f} is the friction force in the telescoping tubes, and $u(t)$ and $\dot{u}(t)$ are the relative displacement and relative velocity, respectively, between joints 2 and 1 in the X direction. The spring force, F_{r}, at joint 2 in the X direction is

$$F_{\mathrm{r}}(t) = k(t)u(t) = [k_e \cos^2 \theta(t)]u(t) \tag{2}$$

where k_e (2984 N/cm) is the stiffness of single spring. The time varying angle θ of the spring elements with respect to horizontal is obtained as $\theta(t) = \sin^{-1}(\alpha - y(t)/L)$, where, $\alpha = 0.917$ is

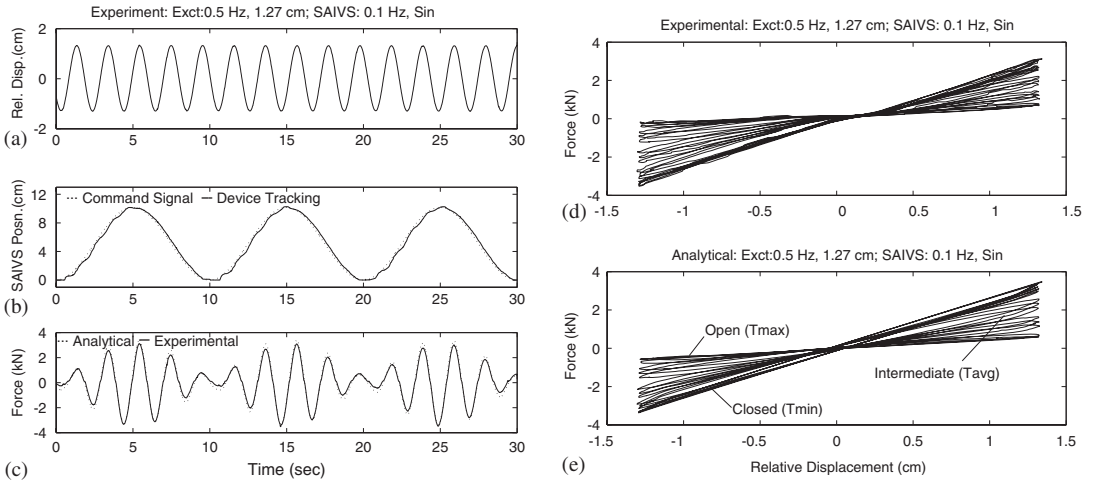

Figure 2. Time histories of: (a) relative displacement; (b) command signal to the SAIVS device and SAIVS position; (c) analytical and experimental force in the SAIVS device; (d) experimental; and (e) analytical force–displacement response of SAIVS device to harmonic excitation of 0.5 Hz: SAIVS switching with a sinusoidal signal of 0.1 Hz.

a non-dimensional constant ($\alpha > y(t)/L$), L is the dimension of an individual spring (15.24cm), and $y(t)$ is the displacement ($L > y(t)$) of joint 1 in the Y direction. Assuming that the velocity $\dot{u}'$, which is along the spring and friction element direction, is equal to $\dot{u}$, for small θ, the friction force at joint 2 in the X direction due to friction in telescoping tubes, F_f, is

$$F_f(t,\dot{u}) = \alpha_f z(\dot{u}')\cos\theta(t) \cong \alpha_f z(\dot{u})\cos\theta(t) \tag{3}$$

where $\alpha_f = 66.88$ N and z is the hysteresis variable [32], which is used to model friction. The variable z is obtained by solving the differential equation [32]: $\dot{z} = (\dot{u} - \gamma|\dot{u}|z|z| - \eta\dot{u}z^2)/Y$, where $\gamma = 0.9$, $\eta = 0.1$ (with $\gamma + \eta = 1$) and $Y = 0.127$cm is the yield displacement. Thus, in the open position, which corresponds to $y(t) = 0$, the device offers minimum stiffness of 373 N/cm (see Figures 2(e) and 3(e)). In the closed position, which corresponds to $y(t) = 10$ cm, the device offers maximum stiffness of 2510 N/cm (see Figures 2(e) and 3(e)). The springs can undergo 2.5 cm of maximum deformation.

Experimental test setup of SAIVS device

The experimental setup to test the force–displacement characteristics of the SAIVS device is shown in Figure 1(d). The SAIVS device is connected between the shake table and a fixed base. The base is fixed by connecting a rod in between a fixed frame and the base. A load cell is connected in series between the connecting rod and the base. The fixed base is supported by four Teflon®-stainless steel sliding bearings. The sliding bearings are supported by four tri-axial load cells, which independently measure friction forces in the bearings. Joints 1, 3 and 4 are connected to carriages which slide on rails. The rails are connected to a plate, which is connected to the fixed base. A linear electromechanical actuator is connected to joint 1 and plate. To measure displacement $y(t)$ of the device, a LVDT is connected to

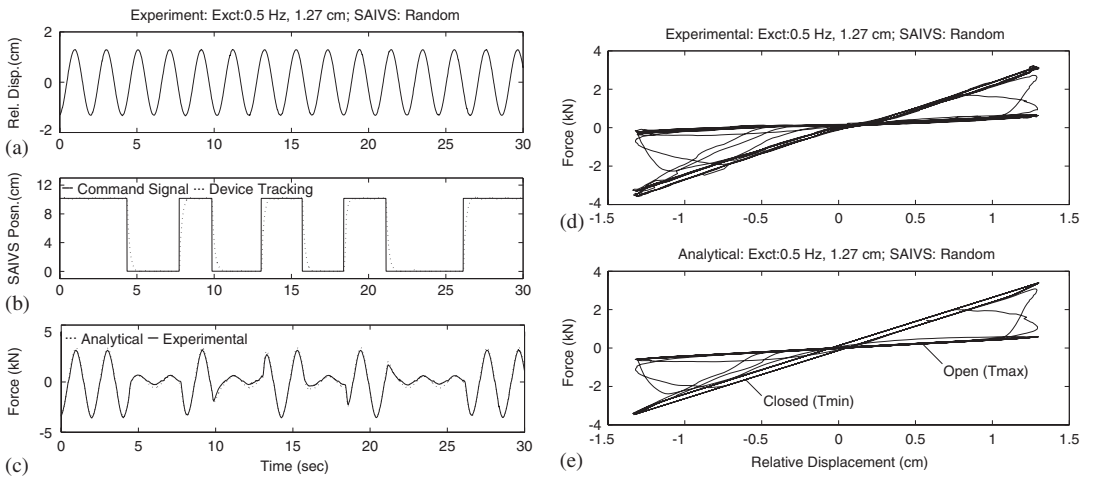

Figure 3. Time histories of: (a) relative displacement; (b) command signal to the SAIVS device and SAIVS position; (c) analytical and experimental force in the SAIVS device; (d) experimental; and (e) analytical force–displacement response of SAIVS device to harmonic excitation of 0.5 Hz: SAIVS Switching with a random command signal.

joint 1. Joint 2 is connected to another carriage/rail assembly, which is connected to the shake table. A servo-hydraulic actuator displaces the shake table based on a prescribed displacement time history of a given test, thus applying a relative displacement between joints 1 and 2 of the device. The SAIVS device acts as a connection between the shake table and the fixed base. The load cell, which is connected between the base and connecting rod, measures the force generated by the SAIVS device and the total friction force in sliding bearings. The force generated by the SAIVS device is obtained by subtracting the friction force, which is measured independently by four tri-axial load cells, from the force measured by the load cell that is connected between the base and connecting rod. The relative displacement, $u(t)$, between joints 1 and 2, is measured by connecting a LVDT between the shake table and the fixed frame.

Analytical and experimental results

A series of tests are performed with harmonic shake table excitation. The SAIVS device position is switched with sinusoidal, square, triangular and random computer command signals. Figures 2(a)–(c) show time histories of the sinusoidal relative displacement of 0.5 Hz frequency, between joints 2 and 1—which is the shake table displacement, SAIVS device switching with a 0.1 Hz sinusoidal electromechanical actuator command signal, and comparison of analytical and experimental SAIVS device force. From Figure 2(b), it is evident that the SAIVS device can track the commanded sinusoidal computer signal satisfactorily. It is evident from Figure 2(c) that the proposed analytical model captures the force generated by the SAIVS device satisfactorily. Figures 2(d) and (e) shows the experimental and analytical force–displacement responses of the SAIVS device switching with sinusoidal command signal. From Figures 2(d) and (e) it is evident that the SAIVS device is capable of varying the

stiffness, continuously and smoothly, between passive open (minimum stiffness) and passive closed (maximum stiffness) positions. The force–displacement behaviour, shown in Figures 2(d) and (e), indicates that the device is capable of generating time varying and non-linear restoring forces. Figures 3(a)–(c) shows relative displacement of 0.5 Hz frequency, SAIVS device switching with a random command signal, and analytical and experimental SAIVS device force time histories. From Figures 3(b) it is evident that the SAIVS device is capable of switching with the commanded random switching signal satisfactorily. Figures 3(d) and (e) shows the experimental and analytical force–displacement behaviour of the SAIVS device switching with random command signal. From Figures 3(d) and (e) it is evident that the device is capable of varying the stiffness continuously and smoothly.

1:5 SCALE SMART SLIDING ISOLATED BUILDING WITH SAIVS DEVICE

As shown in Figures 4(a) and (b) and Table I, a 1:5 scale two-storey building model was designed [31] and built based on laws of artificial mass simulation [33]. Figure 4(a) shows the sliding isolated building model with the SAIVS device. Figure 4(b) shows close up view of the sliding bearings, SAIVS device and passive damper. The SAIVS device is connected between the base of the building and the shake table (see Figure 4(b)). A passive damper is also connected between the base and the shake table (see Figure 4(b)). Weight of each floor is 5.8 kN. Weight of the base is 5.44 kN. The length of the building is 1.47 m, the height is 1.48 m and the width is 0.74 m. The building has a natural period of 0.15 s in the non-isolated case, at model scale, i.e. 0.34 s at prototype scale. The building has a natural period of 1.4 s with the SAIVS device in the passive open position, and 0.53 s with the SAIVS device in the passive closed position in the isolated case, at model scale. Although the closed position represents a very stiff isolation system, it was chosen to use the full stiffness variation range of the SAIVS device. The building model has four sliding bearings, consisting of Teflon-stainless steel interface. The sliding bearings are supported by four tri-axial load cells, which measure frictional forces transmitted from base to the shake table (Figures 4(a) and (b)). The sliding bearings have a dynamic coefficient of friction of 6% at low velocities and 13% at high velocities [17]. A load cell is used to measure forces in the passive damper. The building model is instrumented with LVDTs and accelerometers at base, first, and second floor to measure displacement and acceleration responses. Data acquisition and control is performed using a dSPACE system with MATLAB/Simulink. The block diagram of data acquisition and control system is shown in Figure 4(c). In Figure 4(a), the solid vertical line to the right to which all the arrows point represents fixed reference frame.

EARTHQUAKE EXCITATIONS

To evaluate the effectiveness of the SAIVS device, an analytical and experimental study was performed. Shake table tests were performed under isolated case with: (1) SAIVS device in fixed open position—passive minimum stiffness case, (2) SAIVS device in fixed closed position—passive maximum stiffness case, and (3) semiactive controlled case in which the SAIVS device position is switched in real time based on the developed control algorithm.

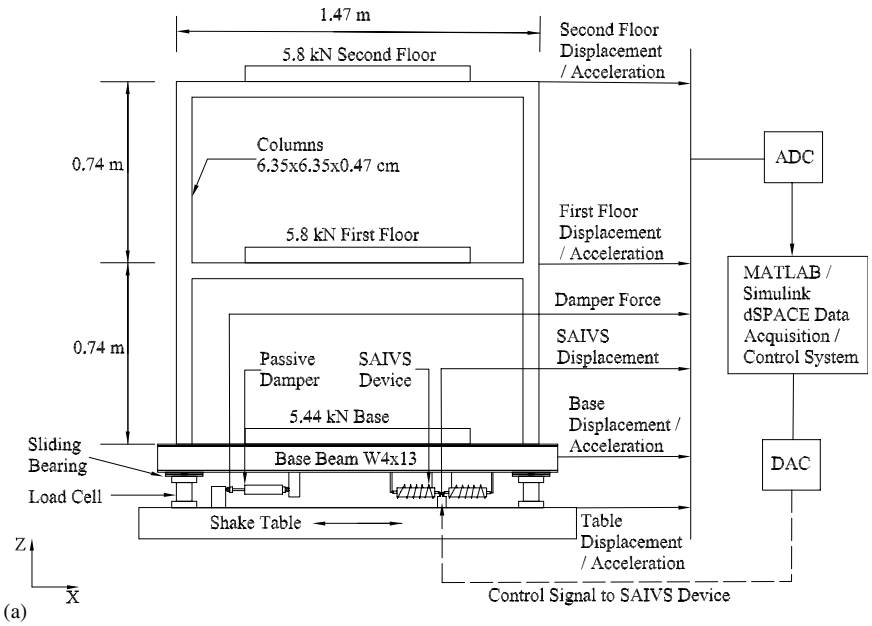

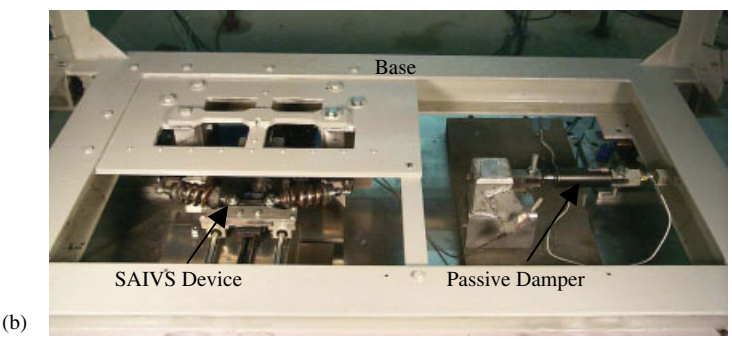

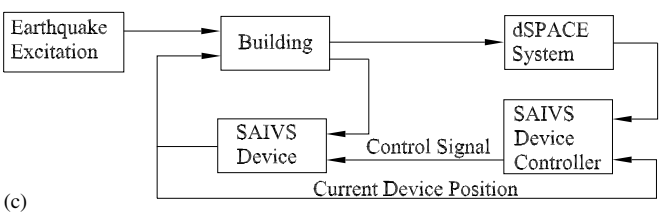

Figure 4. (a) Sliding isolated building model with SAIVS device, (b) close-up view of SAIVS device and passive damper connected between base of the building and shake table; and (c) block diagram of data acquisition and controller.

Table I. Scaling factors.

Parameter	Scaling factor	1:5 Model
Length	l_r	1/5
Time	$\sqrt{l_r}$	$1/\sqrt{5}$
Displacement	l_r	1/5
Velocity	$\sqrt{l_r}$	$1/\sqrt{5}$
Acceleration	1	1
Force	l_r^2	1/25

Shake table tests are performed with following three scaled earthquakes:

(1) El-Centro S00E Earthquake (18 May 1940), peak acceleration: 0.38 g;
(2) Northridge Newhall Earthquake, Channel 1 90° (17 January 1994), peak acceleration: 0.54 g;
(3) Northridge Sylmar Earthquake, Channel 1 90° (17 January 1994), peak acceleration: 0.46 g.

The El Centro earthquake exhibits characteristics of far field motions although it was recorded near fault. Additionally the cases with Newhall (360°—fault normal (FN)), Sylmar (FN), and Kobe (EW and NS) were analytically studied, the results of which are presented in Reference [31]. The analytical study indicated improved performance in semiactive cases over passive cases only under El Centro, Sylmar (90°—fault parallel (FP)), and Newhall (FP) earthquakes. The study with fault normal components of Newhall and Sylmar, and Kobe (EW and NS) earthquakes indicated similar responses in passive and semiactive cases. Hence only the aforementioned three earthquakes were chosen for the experimental study. As per Table I, the earthquake signals were compressed by a time scale factor of $1/\sqrt{5}$.

ANALYTICAL MODEL

The non-linear characteristics of the frictional bearings, passive damper and the SAIVS device are explicitly modelled. Mass of first floor and second floor is $5.92\,\mathrm{N}-\mathrm{s}^2/\mathrm{cm}$. Mass of the base is $5.54\,\mathrm{N}-\mathrm{s}^2/\mathrm{cm}$. The equations of motion are

$$M_2\ddot{U}_2 + C_2(\dot{U}_2 - \dot{U}_1) + K_2(U_2 - U_1) = -M_2\ddot{U}_g \quad (4)$$

$$M_1\ddot{U}_1 + C_1(\dot{U}_1 - \dot{U}_b) + K_1(U_1 - U_b) - C_2(\dot{U}_2 - \dot{U}_1) - K_2(U_2 - U_1) = -M_1\ddot{U}_g \quad (5)$$

$$M_b\ddot{U}_b + \sum_{i=1}^{4} F_{bi} + F_{\mathrm{Damper}} + F_{\mathrm{SAIVS}} - C_1(\dot{U}_1 - \dot{U}_b) - K_1(U_1 - U_b) = -M_b\ddot{U}_g \quad (6)$$

where U_b is the base displacement with respect to shake table, U_1, U_2 are first floor displacement and second floor displacement with respect to shake table, respectively. $\ddot{U}_g$ is the ground acceleration. $\ddot{U}_b, \ddot{U}_1, \ddot{U}_2$ are base, first floor and second floor acceleration, respectively. M_b, M_1, M_2 are the base, first floor and second floor masses, respectively. K_1 is the first floor stiffness, K_2 is the second floor stiffness. C_1 is first floor damping coefficient and C_2 is second

floor damping coefficient. $F_{\mathrm{SAIVS}} = f_{\mathrm{SD}}$ is the force generated by the SAIVS device, which is obtained from Equation (1), by replacing u with U_{b}, which is the base displacement with respect to shake table. The total force in sliding bearings is $f_{\mathrm{s}} = \Sigma F_{\mathrm{b}i}$, $i = 1, 4$, where the force in each sliding bearing is $F_{\mathrm{b}i} = \mu_i w_i z_i$, where μ_i is the coefficient of friction at bearing at location i, w_i is normal load on bearing at location i, z_i is Wen's [32] hysteresis parameter used to model friction. The coefficient of friction [34, 35] at bearing at location i is obtained as $\mu_i = f_{\max\_i} - (f_{\max\_i} - f_{\min\_i})\mathrm{e}^{-(a_i * \mathrm{abs}(\dot{U}_{\mathrm{b}}))}$, where $f_{\max\_i} = 0.13$, $f_{\min\_i} = 0.06$, $a_i = 0.2362\,\mathrm{s/cm}$. The hysteresis variable z [32] is obtained by solving the following differential equation:

$$Y_i \dot{z}_i + \gamma |\dot{U}_{\mathrm{b}}| z_i |z_i| + \eta \dot{U}_{\mathrm{b}} z_i^2 - \dot{U}_{\mathrm{b}} = 0 \tag{7}$$

where $Y_i = 0.127$ cm—small yield displacement of Teflon® before sliding, $\gamma = 0.9$, $\eta = 0.1$. F_{Damper} is the force generated by the passive damper, which is given as

$$f_{\mathrm{c}} = F_{\mathrm{Damper}} = f_{\mathrm{DA}} z + C_{\mathrm{DA}} \dot{U}_{\mathrm{b}} + K_{\mathrm{DA}} U_{\mathrm{b}} \tag{8}$$

where $f_{\mathrm{DA}} = 893.3\,\mathrm{N}$, $C_{\mathrm{DA}} = 19.94\,\mathrm{N-sec/cm}$, and $K_{\mathrm{DA}} = 8.24\,\mathrm{N/cm}$. The hysteresis variable z [32] for the passive damper is obtained by solving differential equation (7) with $Y_i = 0.165\,\mathrm{cm}$.

The state equation, measured output equation, and regulated output equation are:

$$\dot{\mathbf{x}}(t) = \mathbf{A}\mathbf{x}(t) + \mathbf{B}f_{\mathrm{c}}(t) + \mathbf{B}f_{\mathrm{s}}(t) + \mathbf{B}f_{\mathrm{SD}}(t) + \mathbf{E}\ddot{U}_{\mathrm{g}}(t) \tag{9}$$

$$\mathbf{y}(t) = \mathbf{C}_m\mathbf{x}(t) + \mathbf{D}_m f_{\mathrm{c}}(t) + \mathbf{D}_m f_{\mathrm{s}}(t) + \mathbf{D}_m f_{\mathrm{SD}}(t) + \mathbf{E}_m \ddot{U}_{\mathrm{g}}(t) \tag{10}$$

$$\mathbf{z}(t) = \mathbf{C}_z\mathbf{x}(t) + \mathbf{D}_z f_{\mathrm{c}}(t) + \mathbf{D}_z f_{\mathrm{s}}(t) + \mathbf{D}_z f_{\mathrm{SD}}(t) + \mathbf{E}_z \ddot{U}_{\mathrm{g}}(t) \tag{11}$$

where $\mathbf{A}, \mathbf{B}, \mathbf{E}, \mathbf{C}_m, \mathbf{C}_z, \mathbf{D}_m, \mathbf{D}_z, \mathbf{E}_m, \mathbf{E}_z, \dot{\mathbf{x}}(t)$, $\mathbf{x}(\mathbf{t}), \mathbf{y}(\mathbf{t}), \mathbf{z}(\mathbf{t})$ are appropriately defined system matrices or vectors. The equations of motion (Equations (4)–(6)) are solved using an iterative method [34, 35]. The algorithm involves the solution of equations of motion using unconditionally stable Newmark's constant average acceleration method. The solution of differential equations governing the behaviour of the non-linear sliding isolation elements, passive damper and the SAIVS device is obtained using the unconditionally stable semi-implicit Runge–Kutta method. The non-linear forces are moved to the right-hand side as pseudo forces and an iterative procedure consisting of corrective pseudo forces is employed within each time step until equilibrium is achieved.

MOVING AVERAGE NON-LINEAR TANGENTIAL STIFFNESS CONTROL ALGORITHM

From Equation (1) the stiffness variation of the SAIVS device is

$$K_{\mathrm{SAIVS}} = k_e \cos^2\theta(t) \tag{12}$$

Rewriting Equation (12) by including a time delay, τ, we get

$$K_{\mathrm{SAIVS}} = k_e \cos^2\theta(t-\tau) \tag{13}$$

where $K_{\min} < K_{\mathrm{SAIVS}} < K_{\max}$. The time varying angle θ of the springs, with respect to horizontal is obtained as $\theta(t-\tau) = \sin^{-1}(\alpha - y(t-\tau)/L)$, where $\alpha = 0.917$ is a non-dimensional constant

($\alpha > y(t-\tau)/L$), $L = 15.24$ cm is the dimension of an individual spring, and $y(t-\tau)$ is the displacement ($L > y(t-\tau)$) of joint 1, connected to the linear electromechanical actuator. The displacement $y(t-\tau)$ required to control the SAIVS device is

$$y(t-\tau) = \sum_{i=j}^{k} \frac{\gamma}{(k-j)} |U_b(t-\tau_i)|^{\lambda} \tag{14}$$

where $\lambda = 0.6$ is a non-dimensional constant ($\lambda < 1$) and $\gamma = 3.5$ is a constant with appropriate dimension so that $y(t-\tau)$ is in inches, t is the current time ($t \geqslant 0$ and $t > \tau$), $\tau_i = iT_{avg}/100$, and $\tau = jT_{avg}/100$, where T_{avg} is the average period given by Equation (15), $j = 8$ and $k = 18$, and U_b is the relative base displacement with respect to shake table, which can be measured by connecting a LVDT between base and shake table

$$T_{avg} = 2\pi \sqrt{\frac{m_{total}}{(k_{min} + k_{max})/2}} \tag{15}$$

where k_{max} is the maximum stiffness of the SAIVS device (2510 N/cm), k_{min} is the minimum stiffness of the SAIVS device (373 N/cm), and m_{total} is total mass of the system. For $t \leqslant \tau$

$$K_{SAIVS} = k_e \tag{16}$$

The control algorithm (Equation (14)) is designed such that the angle $\theta(t)$ is a non-linear function of the moving average of relative base—shake table displacement; thus making the spring force a non-linear function of the relative base displacement. The non-linear function is designed such that softening tangential stiffness at larger relative displacements is simulated, with eventual negative tangential stiffness at peak relative displacements to reduce the response. A moving average of the relative displacement was chosen to ensure smooth stiffness variation and to reduce the effects of measurement noise. The exponent, $\lambda = 0.6$, was chosen to simulate softening tangential stiffness and was obtained by performing a series of analytical simulations for the chosen earthquakes, which lead to the least response. The coefficient $\gamma = 3.5$ was chosen to ensure that the SAIVS position is within 10 cm, which is the maximum displacement of the device.

RESULTS

Analytical and shake table results in the form of peak values of relative displacements, peak total force at isolation level (total of friction force, SAIVS device force, and passive damper force normalized by total weight), and superstructure accelerations are presented in Table II. Reductions in (1) Newhall 90, (2) Sylmar 90, and (3) El Centro earthquake are notable, hence are presented in detail. Figures 5(a) and (b) present peak experimental relative base displacement with respect to shake table, and peak total force at isolation level, respectively, as a function of peak shake table acceleration, with SAIVS device passive open (minimum stiffness), SAIVS device passive closed (maximum stiffness), and semiactive controlled cases. As evident from Figures 5(a) and (b) and Table II, in Newhall 90 earthquake, the relative base displacement in the passive closed case is reduced by 15%, when compared to the passive open case. However the passive closed case yields 41% increase in total force, when compared with the passive open case. Thus increasing the stiffness in the passive closed

Table II. Comparison of experimental and analytical peak values of responses.

Earthquake	SAIVS device position	Relative (base-shake table) displacement (cm)		Total force at isolation level/weight		Base acceleration (g)		First floor acceleration (g)		Second floor acceleration (g)		First storey drift (cm)		Second storey drift (cm)	
		Expt.	Anly.	Expt.	Anly.	Expt.	Anly.	Expt.	Anly.	Expt.	Anly.	Expt.	Anly.	Expt.	Anly.
Sylmar 90	Open	1.404	1.439	0.251	0.248	0.390	0.540	0.274	0.406	0.507	0.550	0.163	0.137	0.132	0.173
Sylmar 90	Close	1.870	1.730	0.410	0.407	0.470	0.710	0.470	0.550	0.622	0.620	0.237	0.150	0.176	0.175
		(33%)	(20%)	(63%)	(64%)	(21%)	(31%)	(72%)	(35%)	(23%)	(13%)	(45%)	(10%)	(33%)	(1%)
Sylmar 90	Control	1.235	1.146	0.265	0.255	0.420	0.730	0.335	0.510	0.489	0.540	0.190	0.153	0.133	0.170
		(−12%)	(−20%)	(6%)	(3%)	(8%)	(35%)	(22%)	(26%)	(−4%)	(−2%)	(17%)	(12%)	(0%)	(−2%)
Newhall 90	Open	1.787	1.740	0.263	0.252	0.450	0.610	0.288	0.480	0.506	0.630	0.175	0.133	0.155	0.186
Newhall 90	Close	1.525	1.590	0.370	0.398	0.610	0.780	0.414	0.780	0.705	0.770	0.277	0.178	0.203	0.225
		(−15%)	(−9%)	(41%)	(58%)	(36%)	(28%)	(44%)	(63%)	(39%)	(22%)	(58%)	(34%)	(31%)	(21%)
Newhall 90	Control	1.160	1.150	0.270	0.280	0.490	0.710	0.316	0.524	0.510	0.700	0.184	0.152	0.178	0.217
		(−35%)	(−34%)	(3%)	(11%)	(9%)	(16%)	(10%)	(9%)	(0%)	(11%)	(5%)	(14%)	(15%)	(17%)
El Centro	Open	0.768	0.792	0.210	0.227	0.320	0.630	0.287	0.460	0.395	0.530	0.129	0.124	0.150	0.159
El Centro	Close	1.058	1.020	0.308	0.322	0.390	0.850	0.334	0.660	0.498	0.613	0.161	0.147	0.162	0.171
		(38%)	(29%)	(47%)	(42%)	(22%)	(35%)	(16%)	(43%)	(26%)	(16%)	(25%)	(19%)	(8%)	(8%)
El Centro	Control	0.696	0.756	0.239	0.241	0.350	0.580	0.271	0.461	0.352	0.571	0.120	0.130	0.156	0.167
		(−9%)	(−5%)	(14%)	(6%)	(9%)	(−8%)	(−6%)	(0%)	(−11%)	(8%)	(−7%)	(5%)	(4%)	(5%)

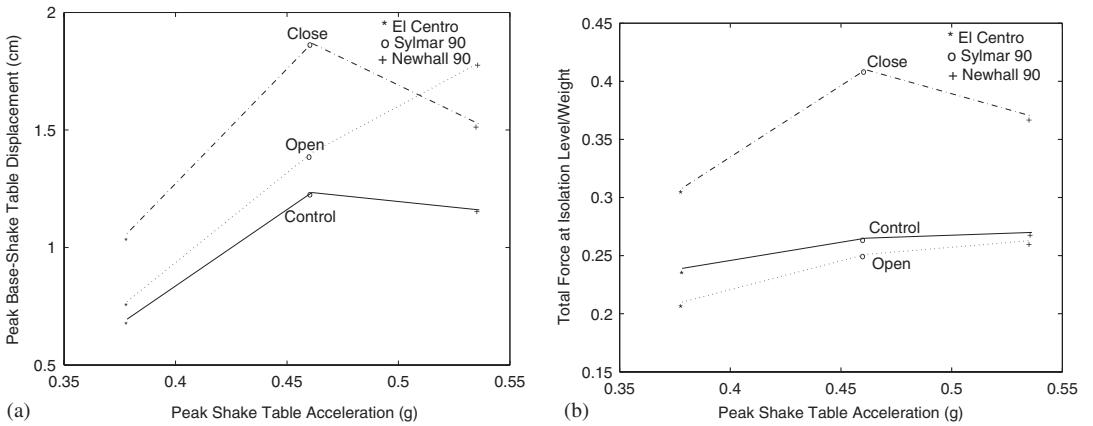

Figure 5. Comparison of peak experimental: (a) relative base–shake table (ground) displacement response; and (b) total force at isolation level/weight as a function of peak shake table (ground) acceleration under various earthquakes.

case attracts more forces. The semiactive controlled case, shown in Figures 5(a) and (b) and Table II, further reduces the relative base displacement by 24% when compared with the passive closed case, while maintaining the total force at isolation level close to the passive open case. The smart variation of stiffness in the controlled case results in the least relative base displacement response, when compared with the passive open and passive closed cases, while maintaining the isolation level forces at the same level as the passive open case. From Table II, a similar set of observations can be obtained from the analytical results under Newhall 90 as well. Thus, reductions in both the displacements and forces reveal the effectiveness of variable stiffness system provided by the SAIVS device. Table II also presents the peak values of experimental and analytical interstorey drifts and superstructure accelerations under Newhall 90. The passive closed case, as a result of increased forces, results in increased interstorey drifts and superstructure accelerations when compared with the passive open case. The controlled case, however, maintains interstorey drifts and superstructure accelerations within bounds of the passive open and passive closed cases. Note that in Newhall 90 there is 10% increase in the base and first floor acceleration in the controlled case when compared to the passive open case (see Table II). However, there is a 35% decrease in base displacement in the controlled case when compared to the passive open case. If the seismic gap is inadequate to accommodate such increased base displacements as in the passive open case then the resulting impact response will be undesirable, thus undermining the beneficial effects of sliding isolation system [4]. The semiactive controlled case achieves the important objective of reducing the base displacement response (avoiding potential impact) while maintaining the base and first floor accelerations within bounds of passive open and closed cases. In the case of sliding isolated structures with lower friction ($\mu = 0.05$) the base displacement in the passive open case will be excessive, in which case, semiactive control would be of significant benefit.

Figures 5(a) and (b) and Table II also present the measured responses under Sylmar 90 and El Centro earthquake. In both the earthquakes, the controlled case yields the least relative base displacement response, when compared with the passive open and passive closed cases.

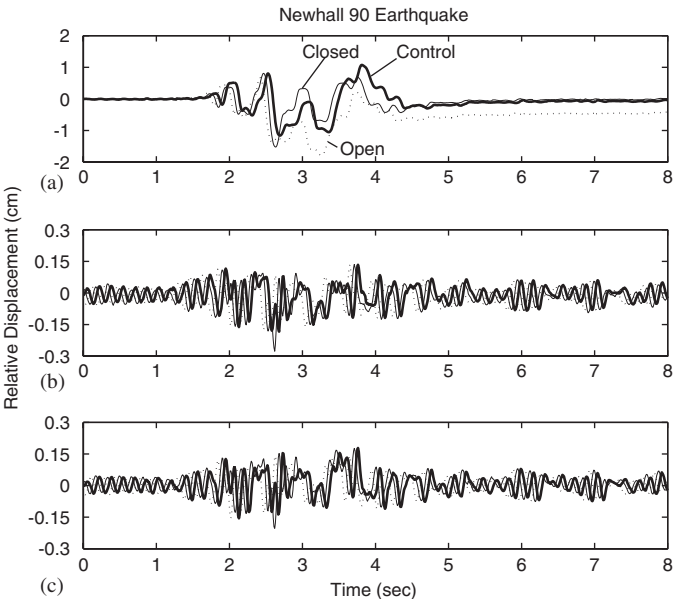

Figure 6. Experimental relative displacement time history responses under Newhall 90 earthquake: (a) base-ground; (b) first floor-base; and (c) second floor-first floor.

Under Sylmar 90, the controlled case reduces the relative base displacement by 12% when compared with the passive open case, and by 34% when compared with the passive closed case. Under El Centro, the controlled case results in 9% reduction in relative base displacement when compared with the passive open case, and 34% reduction in relative base displacement when compared with the passive closed case. Under Sylmar 90 and El Centro, the controlled case also maintains the isolation level forces close to the passive open case. Note that the maximum relative base displacement response under Sylmar 90 and El Centro earthquakes occur in the passive closed case; whereas, under Newhall 90 earthquake it occurs in the passive open case. However, the semiactive controlled case—due to the smart variation of stiffness—reduces the relative base displacements further than the passive open and closed cases in all earthquakes, while maintaining the isolation level forces close to the passive open case. Thus the SAIVS device, along with the developed control algorithm, reduces displacements and forces effectively. From Table II, it is evident that under Sylmar 90 and El Centro earthquakes the passive closed case results in the increased superstructure accelerations and interstorey drifts, when compared to the passive open case. The controlled case, however, maintains the superstructure accelerations and interstorey drifts within bounds of the passive open and closed case, under both the earthquakes.

Figures 6–13 present the shake table test results in the form of relative displacement time histories, total force at the isolation level normalized by total weight as a function of relative base displacement, SAIVS device force normalized by total weight as a function of relative base displacement, and SAIVS device position and second floor acceleration time histories under Newhall 90 and Sylmar 90 earthquakes. Note that in Figures 6 and 10 a 0.05 s time shift is introduced in the comparison of relative displacement time histories in order

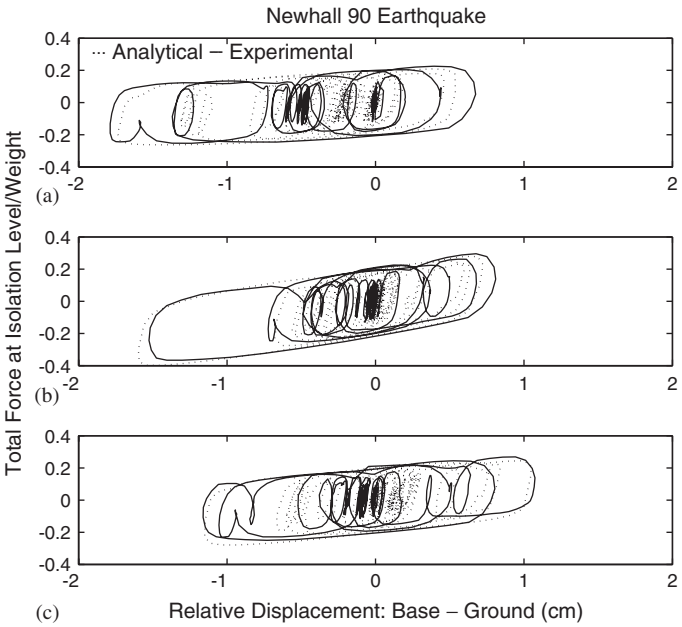

Figure 7. Comparison of experimental and analytical total force at isolation level/weight as a function of relative base displacement under Newhall 90 earthquake: (a) SAIVS open; (b) SAIVS close; and (c) SAIVS control.

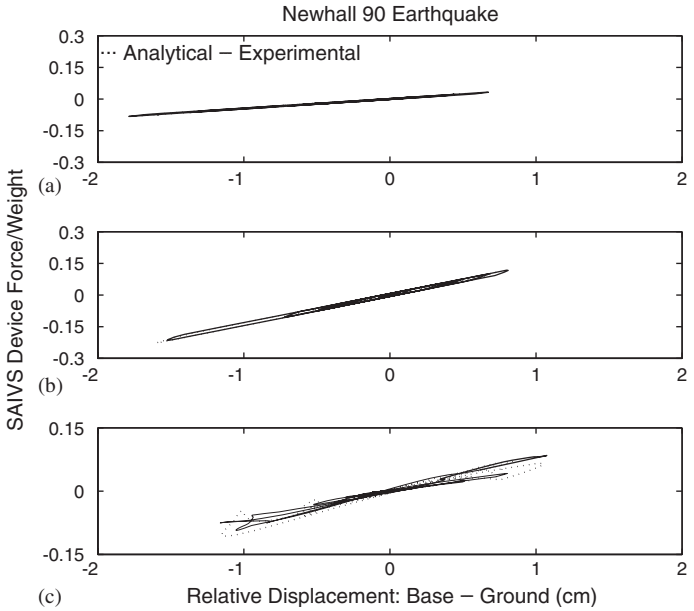

Figure 8. Comparison of experimental and analytical SAIVS device force/weight as a function of relative base displacement under Newhall 90 earthquake: (a) SAIVS open; (b) SAIVS close; and (c) SAIVS control.

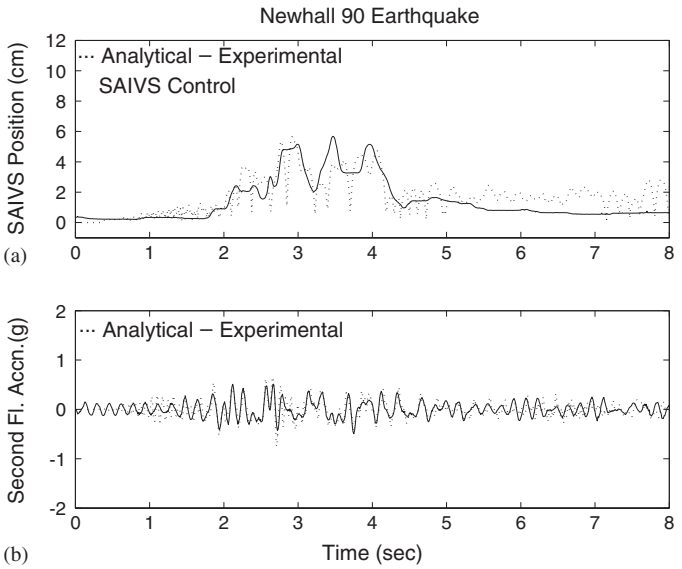

Figure 9. (a) Comparison of analytical and experimental SAIVS switching, and (b) analytical and experimental second floor acceleration time histories under Newhall 90 earthquake.

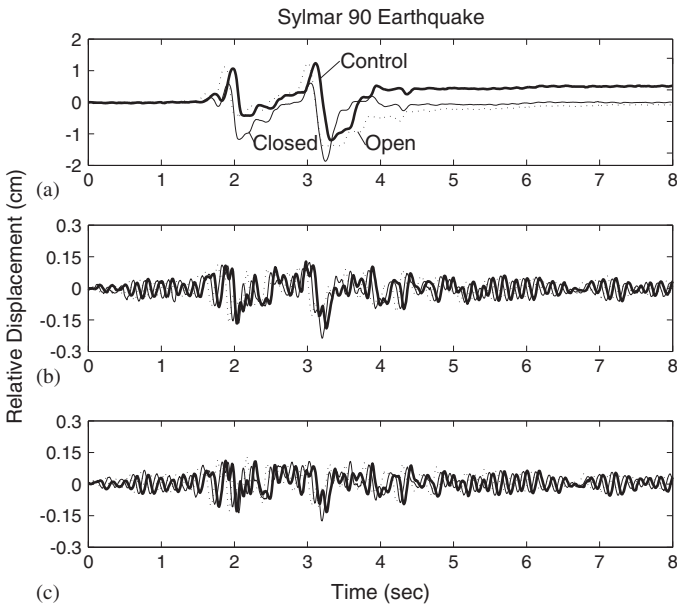

Figure 10. Experimental relative displacement time history responses under Sylmar 90 earthquake: (a) base-ground; (b) first floor-base; and (c) second floor-first floor.

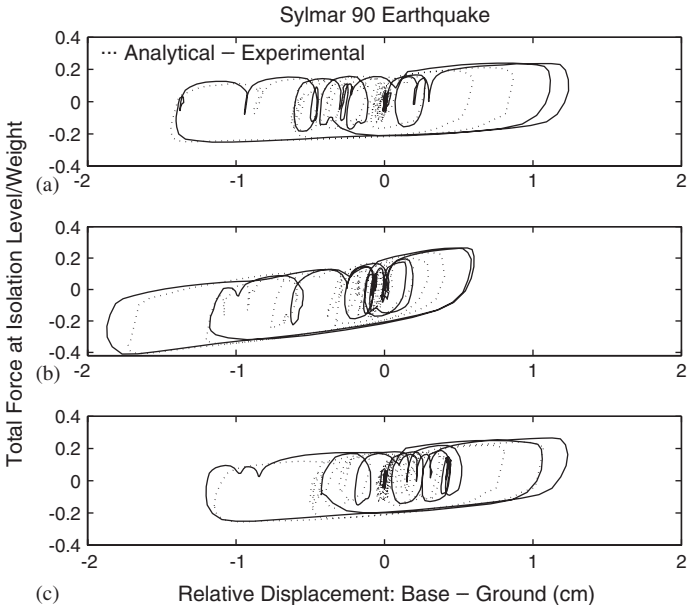

Figure 11. Comparison of experimental and analytical total force at isolation level/weight as a function of relative base displacement under Sylmar 90 earthquake: (a) SAIVS open; (b) SAIVS close; and (c) SAIVS control.

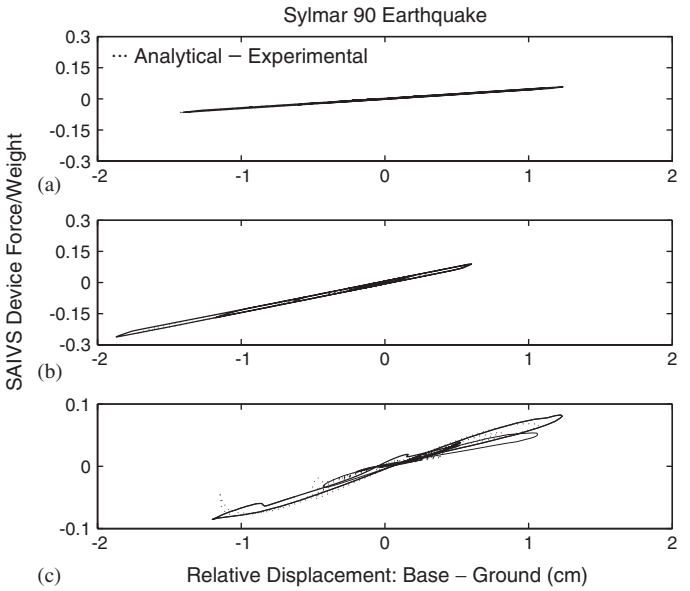

Figure 12. Comparison of experimental and analytical SAIVS device force/weight as a function of relative base displacement under Sylmar 90 earthquake: (a) SAIVS open; (b) SAIVS close; and (c) SAIVS control.

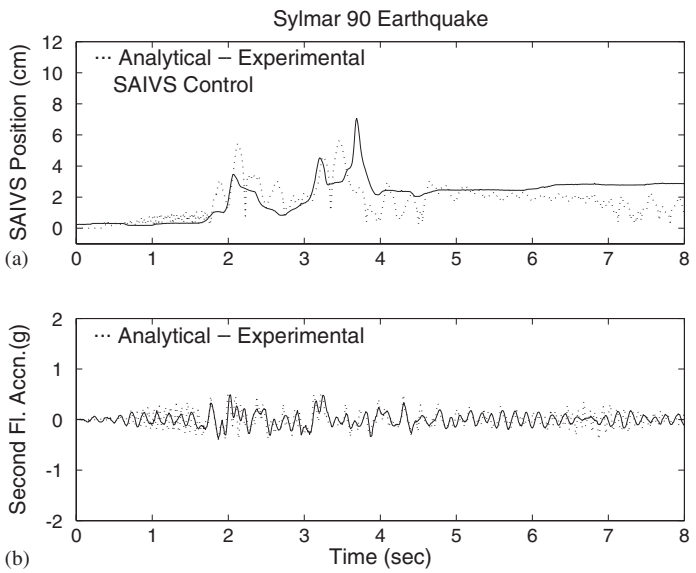

Figure 13. (a) Comparison of experimental and analytical SAIVS switching and (b) second floor acceleration time histories under Sylmar 90 earthquake.

to highlight the differences clearly. Figures 7–9 and 11–13 also present the corresponding analytical results. From the comparison of experimental relative displacement time histories under Newhall 90 earthquake, presented in Figure 6, it is evident that most of the displacement occurs at the isolation level and interstorey drifts are significantly reduced. Figure 7 presents the analytical and experimental total force at the isolation level as a function of relative base displacement loops under Newhall 90 earthquake, with passive open, passive closed, and semiactive controlled cases. From Figure 7 it is evident that the controlled case reduces the relative base displacement further than the passive open and passive closed cases, while maintaining isolation level forces close to the passive open case. The comparison of analytical and experimental results, presented in Figure 7, indicate that the analytical model captures the response of the sliding isolated building model satisfactorily. Figure 8 presents the SAIVS device force normalized by total weight as a function of relative base displacement under Newhall 90 earthquake, with passive open, passive closed, and semiactive controlled cases. Note from Figures 8(a) and (b), the stiffness of the sliding isolation system does not change in the passive open and passive closed cases. Whereas in the controlled case, presented in Figure 8(c), the SAIVS device varies the stiffness, hence the period of the isolation system, continuously and smoothly as commanded by the control algorithm. This intelligent variation of the period of the sliding isolation system by the SAIVS device yields reductions in displacements and forces. The softening tangential stiffness is evident in analytical and experimental force–displacement loops (see Figure 8(c)); however, the eventual negative stiffness is evident only in analytical force–displacement loops at peak relative displacements. The reduction in response is primarily due to the softening tangential stiffness (see Figure 8(c)), which prevents the excessive strain energy from being stored in the SAIVS device at larger displacements. This softening tangential stiffness coupled with energy dissipation

results in an efficient system. This is evident in Figures 6(a) and 9(a), wherein when the peak relative displacement occurs at 2.7 s the stiffness of the device is smaller, following which the stiffness increases when the relative displacement is smaller. The analytical and experimental SAIVS device switching and second floor acceleration time histories in the controlled case, under Newhall 90 earthquake, are presented in Figure 9. The second floor acceleration time histories, presented in Figure 9(b), reveal that no abrupt acceleration spikes occur as the SAIVS device varies the stiffness continuously and smoothly (see Figure 8(c)). A similar set of observations, as in Newhall 90 earthquake, can be obtained from the response plots under Sylmar 90 earthquake presented in Figures 10–13. The softening tangential stiffness at 3.3 s (see Figures 10(a) and 13(a)), when the peak relative displacement occurs, followed by eventual negative stiffness seen in the analytical force–displacement loops (see Figure 12(c)) is the primary reason for response reduction. From the peak values of responses presented in Table II and comparison of analytical and experimental results presented in Figures 7–9 and 11–13, it is evident that the analytical model captures the overall response behaviour of the building model satisfactorily.

Thus from the analytical and experimental study it can be concluded that the semiactive SAIVS device, as a result of continuous and smooth variation of the stiffness—hence the period—of the sliding base isolation system, reduces the base displacements further than the passive open and passive closed cases, while maintaining isolation level forces close to the passive open case.

CONCLUSIONS

The analytical and experimental study presented clearly indicates that the semiactive stiffness variation using the SAIVS device in sliding base isolation systems in buildings reduces the base displacements further than the passive open and passive closed cases, while maintaining isolation level forces close to the passive open case. Whereas, in base isolated buildings, increasing stiffness at the isolation level (i.e. passive closed case) does not necessarily reduce bearings displacements. Increased passive isolation stiffness certainly results in increased superstructure accelerations and drifts, thus undermining the beneficial effects of sliding isolation system. One of the main reasons for the superior performance of the semiactive case is the ability of the proposed new controller and the SAIVS device to vary the stiffness continuously and smoothly, thus varying the period of the smart sliding isolated structure. The developed non-linear analytical model captures the overall behaviour of the smart sliding base isolated building model satisfactorily. While the results shown herein demonstrate the potential of the variable stiffness system in fault parallel components of chosen earthquakes, better control algorithms need to be developed for achieving reductions in response in the case of fault normal components. The analytical and experimental study demonstrates the significant potential of the SAIVS system.

ACKNOWLEDGEMENTS

This project was funded by the National Science Foundation under grant NSF-CAREER Grant Number CMS-9996290, which is gratefully acknowledged.

REFERENCES

1. Kelly JM. *Earthquake-resistant Design with Rubber* (2nd edn). Springer: New York, 1997.
2. Chopra AK. *Dynamics of Structures*: *Theory and Applications to Earthquake Engineering* (2nd edn). Prentice Hall: New York, 2002.
3. Hall JF, Heaton TH, Halling MW, Wald DJ. Near source ground motion and its effects on flexible buildings. *Earthquake Spectra* 1995; **11**(4):569–605.
4. Nagarajaiah S, Sun X. Base-isolated FCC building: impact response during Northridge earthquake. *Journal of Structural Engineering* 2001; **127**(9):1063–1074.
5. Asher JW, Young RP, Ewing RD. Seismic isolation design of the San Bernardino county medical center replacement project. *The Structural Design of Tall Buildings* 1996; **5**:265–279.
6. Kelly JM. The role of damping in seismic isolation. *Earthquake Engineering and Structural Dynamics* 1999; **28**(1):3–20.
7. Hall JF. Discussion of 'The role of damping in seismic isolation'. *Earthquake Engineering and Structural Dynamics* 1999; **28**(12):1717–1720.
8. Wolff ED, Constantinou MC. Experimental study of seismic isolation systems with emphasis on secondary system response and verification of accuracy of dynamic response history analysis methods. *Report No. MCEER-04-0001*, Multidisciplinary Center for Earthquake Engineering Research, State University of New York, Buffalo, NY, 2004.
9. Spencer BF, Nagarajaiah S. State of the art structural control. *Journal of Structural Engineering* 2003; **129**(7):845–856.
10. Nagarajaiah S. Fuzzy controller for structures with hybrid isolation system. *Proceedings of First World Conference on Structural Control*, vol. TA2, University of Southern California, California, August 1994; 67–76.
11. Carlson JD, Chrzan MJ. Magnetorheological fluid dampers. *U.S. Patent #5,277,281*, 1994.
12. Spencer BF, Dyke SJ, Sain MK, Carlson JD. Phenomenological model of a magnetorheological damper. *Journal of Engineering Mechanics* 1997; **123**(3):230–238.
13. Spencer BF, Johnson EA, Ramallo JC. Smart isolation for seismic control. *JSME International Journal Series*, C 2000; **43**(3):704–711.
14. Ramallo JC, Johnson EA, Spencer BF. Smart base isolation systems. *Journal of Engineering Mechanics* 2002; **128**(10):1088–1099.
15. Yoshioka H, Ramallo JC, Spencer BF. Smart base isolation strategies employing magneto-rheological damper. *Journal of Structural Engineering* 2002; **128**(5):540–551.
16. Sahasrabudhe S, Nagarajaiah S. Experimental study of sliding base-isolated buildings with magnetorheological dampers in near-fault earthquakes. *Journal of Structural Engineering* 2005; **131**(7):1025–1034.
17. Sahasrabudhe S, Nagarajaiah S. Semi-active control of sliding isolated bridges using MR dampers: an experimental and numerical study. *Earthquake Engineering and Structural Dynamics* 2005; **34**(8):965–983.
18. Makris N. Rigidity-plasticity-viscosity: can electrorheological dampers protect base isolated structures from near source ground motions? *Earthquake Engineering and Structural Dynamics* 1997; **26**(5):571–591.
19. Gavin HP. Control of seismically excited vibration using electrorheological materials and Lyapunov methods. *IEEE Transactions on Automatic Control* 2001; **9**(1):27–36.
20. Kurata N, Kobori T, Takahashi M, Niwa N, Hiroshi M. Actual seismic response controlled building with semiactive damper. *Earthquake Engineering and Structural Dynamics* 1999; **28**(11):1427–1447.
21. Gavin HP, Alhan C, Oka N. Fault tolerance of semi-active seismic isolation. *Journal of Structural Engineering* 2003; **129**(7):922–932.
22. Symans MD, Kelly SW. Fuzzy logic control of bridge structures using intelligent semiactive seismic isolation system. *Earthquake Engineering and Structural Dynamics* 1999; **28**(1):37–60.
23. Madden GJ, Wongprasert N, Symans MD. Analytical and numerical study of a smart sliding isolation system for seismic protection of buildings. *Computer Aided Civil and Infrastructure Engineering* 2003; **18**(1):19–30.
24. Nagarajaiah S, Riley MA, Reinhorn AM. Control of sliding isolated bridge with absolute acceleration feedback. *Journal of Engineering Mechanics* 1993; **119**(11):2317–2332.
25. Kobori T, Takahashi M, Nasu T, Niwa N, Ogasawara K. Seismic response controlled structure with active variable stiffness system. *International Journal on Earthquake Engineering and Structural Dynamics* 1993; **22**(9):925–941.
26. Nasu T, Kobori T, Takahashi M, Niwa N, Ogasawara K. Active variable stiffness system with non-resonant control. *Earthquake Engineering and Structural Dynamics* 2001; **30**(11):1597–1614.
27. Yang JN, Kim JH, Agrawal A. Resetting semiactive stiffness damper for seismic response control. *Journal of Structural Engineering* 2000; **126**(12):1427–1433.
28. Jabbari F, Bobrow J. Vibration suppression with resettable device. *Journal of Engineering Mechanics* 2002; **128**(9):916–924.
29. Nagarajaiah S, Mate D. Semi-active control of continuously variable stiffness system. *Proceedings Second World Conference on Structural Control*, vol. 1, Kyoto, Japan, July 1998; 397–406.

30. Narasimhan S, Nagarajaiah S. A STFT semiactive controller for base isolated buildings with variable stiffness isolation systems. *Engineering Structures* 2005; **27**(4):514–523.
31. Sahasrabudhe S. Semi-active control of sliding isolated buildings and bridges with variable stiffness and damping systems. *Ph.D. Thesis*, Rice University, Houston, TX, USA, 2002.
32. Wen YK. Method of random vibration of hysteretic systems. *Journal of Engineering Mechanics* 1976; **102**(2):249–263.
33. Mills RS, Krawinkler H, Gere JM. Model tests on earthquake simulators development and implementation of experimental procedures. *Report No. 39*, John A. Blume Earthquake Engineering Center, Stanford University, 1979.
34. Nagarajaiah S, Reinhorn AM, Constantinou MC. 3D-BASIS: nonlinear dynamic analysis of three-dimensional base isolated structures—Part II. *Report No. NCEER-91-0005*, National Center for Earthquake Engineering Research, SUNY, Buffalo, NY 1991.
35. Nagarajaiah S, Reinhorn AM, Constantinou MC. Nonlinear dynamic analysis of 3D-base isolated structures. *Journal of Structural Engineering* 1991; **117**(7):2035–2054.

